RESEARCH ARTICLE SUMMARY

NATURAL PRODUCTS

Autologous DNA mobilization and multiplication expedite natural products discovery from bacteria

Feng Xie†, Haowen Zhao†, Jiaqi Liu, Xiaoli Yang, Markus Neuber, Amay Ajaykumar Agrawal, Amninder Kaur, Jennifer Herrmann, Olga V. Kalinina, Xiaoyi Wei, Rolf Müller*, Chengzhang Fu*

INTRODUCTION: The escalation of antimicrobial resistance as a global health threat is driven by highly effective genetic spreading mechanisms. Antibiotic resistance gene transmission involves a multistep process: mobilization through insertion sequences or integrons, relocation from chromosomes to mobile genetic elements, and lastly, horizontal gene transfer among microorganisms. We aimed to artificially mimic this mechanism to facilitate the "mobilization-relocation-transfer" process for large DNA fragments in bacteria, such as biosynthetic gene clusters (BGCs) responsible for producing natural products.

RATIONALE: We developed ACTIMOT (Advanced Cas9-mediaTed In vivo MObilization and mulTiplication of BGCs) to mobilize, relocate, and multiply BGCs within bacterial cells. We used clustered regularly interspaced short palindromic repeats (CRISPR) and the CRISPR-associated protein 9 (Cas9) to liberate large target DNA regions and translocated the liberated BGCs onto a plasmid through homologous recombination, enabling its multiplication within the same cell. This BGC amplification holds immense potential to enhance natural product production, thus leading to the discovery of unknown compounds.

RESULTS: We designed two sets of plasmids: the pRel series for BGC mobilization and the pCap series for BGC relocation and multiplication. As a proof of concept, we engineered two plasmids targeting the 24-kb actinorhodin BGC (*Act*) in *Streptomyces coelicolor* M145. After conjugations, we obtained pCap-*Act* and observed production enhancement of actinorhodin in the *Act*-mobilized mutant, demonstrating ACTIMOT's feasibility.

Expanding our approach, we applied ACTIMOT to the 48-kb target DNA region *Sav11* from *S. avidinii* DSM40526, containing two unknown nonribosomal peptide synthetase (NRPS) BGCs. Using the improved single-plasmid ACTIMOT devised by merging pRel and pCap, we enhanced efficiency and indeed identified two previously unknown peptide families: avidistatins (**1** to **7**) and avidilipopeptides (**8** to **22**). Additionally, we applied ACTIMOT to the 67-kb *Sar13*, housing a cryptic "ladderane"-NRPS BGC from *S. armeniacus* DSM19369. The corresponding BGC activation led to a 40-fold production increase in mobilipeptin (**23** to **27**) production, including their cryptic cyclic peptide precursor, providing insights into the biosynthesis of the "ladderane"-NRPS BGC family.

Furthermore, applying ACTIMOT to the 149-kb *Sav17* from *S. avidinii* DSM40526 led to the discovery of benzoxazole-containing actimotins (**29** to **40**). Actimotins are produced by a currently unpredictable BGC located within *Sav17*, highlighting ACTIMOT's potential for unraveling unrecognized pathways. Although an initial panel of cell-based bioactivity assays did not detect substantial activity for most compounds, actimotin J exhibited decent transthyretin-stabilizing activity in a range similar to that of the approved drug tafamidis, suggesting that additional activity screening assays may uncover bioactivities of compounds discovered by ACTIMOT.

CONCLUSION: Using ACTIMOT, we uncovered four uncharacterized natural compound classes without the need for altering native BGCs. ACTIMOT effectively mobilizes and multiplies BGCs, directly augmenting compound yields within native species through the gene dosage effect, as demonstrated by the discoveries of mobilipeptins and actimotins. When BGCs are repressed in the native strains, relocated BGCs can be transferred to genetically tractable hosts for production, exemplified by avidistatins and avidilipopeptins. Future research will explore ACTIMOT's adaptability in other species and its potential to unlock the vast genomic potential within natural product factories. Overall, this work highlights the promise of ACTIMOT in accelerating natural product discovery. ■

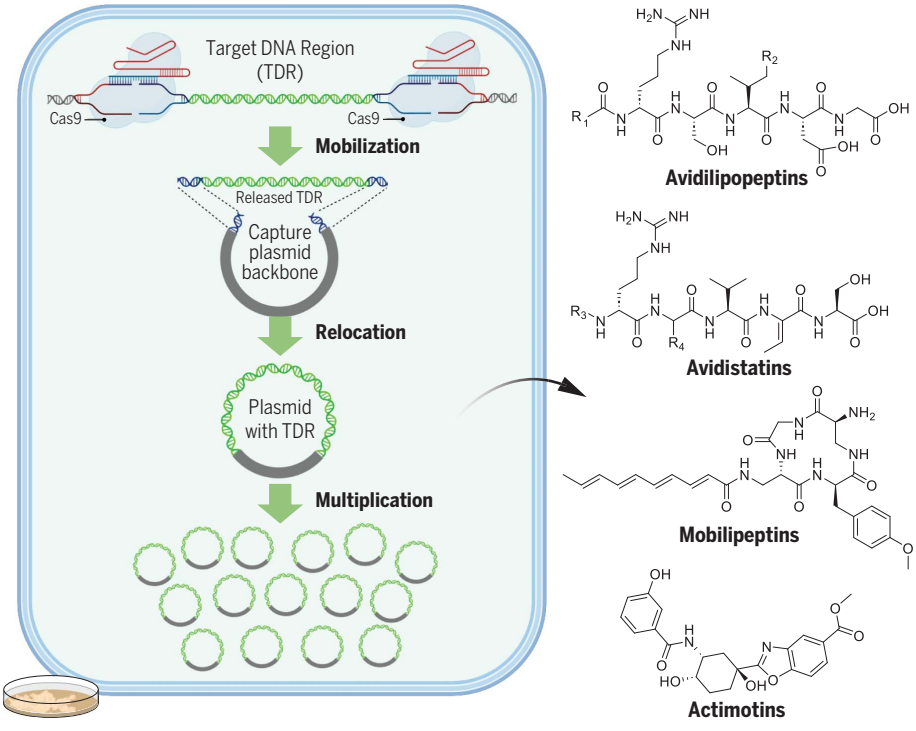

ACTIMOT facilitates the exploration of cryptic biosynthetic potential in bacteria. ACTIMOT leverages CRISPR-Cas9 to efficiently mobilize and relocate the target DNA region harboring BGC(s) onto a multicopy plasmid backbone, enabling BGC(s) multiplication. This process allows product yield enhancement within native host cells. Using ACTIMOT has led to the discovery of four classes of previously unknown compounds. [Figure partially created with BioRender.com]

The list of author affiliations is available in the full article online.
*Corresponding author. Email: rolf.mueller@helmholtz-hips.de (R.M.); chengzhang.fu@helmholtz-hips.de (C.F.)
†These authors contributed equally to this work.
Cite this article as F. Xie *et al.*, *Science* **386**, eabq7333 (2024). DOI: 10.1126/science.abq7333

READ THE FULL ARTICLE AT
https://doi.org/10.1126/science.abq7333

RESEARCH ARTICLE

NATURAL PRODUCTS

Autologous DNA mobilization and multiplication expedite natural products discovery from bacteria

Feng Xie[1,2,3]†, Haowen Zhao[1,2,3]†, Jiaqi Liu[1,2], Xiaoli Yang[1,2], Markus Neuber[1], Amay Ajaykumar Agrawal[1], Amninder Kaur[1,2,3], Jennifer Herrmann[1,3], Olga V. Kalinina[1,3,4], Xiaoyi Wei[5], Rolf Müller[1,2,3,6,7]*, Chengzhang Fu[1,2,3]*

The transmission of antibiotic-resistance genes, comprising mobilization and relocation events, orchestrates the dissemination of antimicrobial resistance. Inspired by this evolutionarily successful paradigm, we developed ACTIMOT, a CRISPR-Cas9–based approach to unlock the vast chemical diversity concealed within bacterial genomes. ACTIMOT enables the efficient mobilization and relocation of large DNA fragments from the chromosome to replicative plasmids within the same bacterial cell. ACTIMOT circumvents the limitations of traditional molecular cloning methods involving handling and replicating large pieces of genomic DNA. Using ACTIMOT, we mobilized and activated four cryptic biosynthetic gene clusters from *Streptomyces*, leading to the discovery of 39 compounds across four distinct classes. This work highlights the potential of ACTIMOT for accelerating the exploration of biosynthetic pathways and the discovery of natural products.

The antimicrobial resistance (AMR) crisis has been identified by the World Health Organization (WHO) as one of the greatest global threats (*1*). Although AMR undoubtedly poses a major health threat, its inherent evolutionary mechanism in gene transmission appears to be a successful strategy in nature. Recent studies have indicated that the spread of antibiotic-resistance genes (ARGs) occurs through the transfer of AMR genes from the chromosome to mobile genetic elements (MGEs) such as multicopy plasmids (*2*, *3*). This process generally includes two successive events: the mobilization of ARGs typically achieved by either insertion sequences (*4*, *5*) or integrons (*6*, *7*) and the subsequent relocation of the mobilized ARGs to MGEs (*8*). Subsequently, horizontal gene transfer (HGT) facilitates the transmission of ARGs among bacteria (*2*, *3*) (Fig. 1A).

Inspired by the "mobilization-relocation-transfer" process naturally occurring during AMR spread, we contemplated the possibility of artificially simulating the molecular mechanisms to mobilize and transmit large DNA fragments, a fundamental requirement for numerous potential applications. For instance, biosynthetic gene clusters (BGCs)—composed of multiple genes (varying from several kb to >100 kb) forming a pathway to produce small molecules and related congeners—hold immense value for chemical entities exhibiting extremely diverse biological activities. Such natural products (NPs) have contributed to 66.8% of all US Food and Drug Administration (FDA)–approved small-molecule drugs in the last four decades, making them vital for the treatment of various diseases (*9*). However, technical challenges and high rediscovery rates have led to a decline in interest from the pharmaceutical industry in NP research (*10*). Nevertheless, recent genomic investigations have unveiled the heavily underestimated potential of untapped secondary metabolites in bacteria, even in extensively studied taxa such as *Actinobacteria* (*11*). Although prior efforts in the field developed different strategies to uncover NPs from BGCs (*12*–*21*), the disconnection between the enormous biosynthetic potential of BGCs and our limited knowledge of encoded chemical entities highlights the need for alternative approaches to accelerate the discovery of what are now known as "cryptic" NPs (*22*).

To accomplish this objective, we have devised an approach inspired by ARG transmission called ACTIMOT (Advanced Cas9-mediaTed In vivo MObilization and mulTiplication of BGCs). To simulate the mechanisms of gene mobilization, we have leveraged the power of clustered regularly interspaced short palindromic repeats (CRISPR) and the CRISPR-associated protein 9 (Cas9) (*23*–*27*), a cutting-edge genome-editing technology, to artificially liberate large target DNA regions (TDRs) such as BGCs from the bacterial chromosome (Fig. 1B). Subsequently, the Cas9-cleaved TDR is captured by a multicopy plasmid within the cell, mimicking the relocation process (Fig. 1B). The presence of the multicopy replicon enables the multiplication of the target BGC, resembling another crucial mechanism of AMR occurrence, namely gene duplication and amplification (*28*). ACTIMOT allows for a cloning process independent of genomic DNA isolation and intermediate cloning hosts, which enhances the efficiency of relocating the BGC into a plasmid within the native cell, thereby facilitating the discovery of the final products through the gene amplification effect. In cases where gene dosage does not increase production, the mobilized BGCs are transferred into heterologous hosts, thus circumventing negative regulation in the native host. In this study, we present the development and successful application of ACTIMOT, directly enabling the discovery of four classes of previously unknown NPs without additional pathway engineering.

The principle and design of ACTIMOT

In contrast to conventional molecular cloning, ACTIMOT eliminates the need for isolating genomic DNA from the source species and replicating recombinant DNA in the host species. Instead, ACTIMOT enables the leap of TDRs from the bacterial chromosome to plasmids within the same bacterial cell. We developed the prototype of ACTIMOT as comprising two distinct *Streptomyces*–*Escherichia coli* shuttle plasmids, facilitating TDR mobilization and relocation. The release plasmid (pRel) used in the TDR mobilization step consists of a codon-optimized *Cas9* gene, a single-guide RNA (sgRNA) cassette, and a *Streptomyces* replicon [from pSG5 (*29*)]. The capture plasmid (pCap) for BGC relocation features a bacterial artificial chromosome (BAC) backbone and a *Streptomyces*-specific replicon [either from pSG5 or pIJ101 (*30*)] (Fig. 2A, figs. S1 and S2, and table S2). The option of the pIJ101 replicon in pCap ensures compatibility with pRel when used together in *Streptomyces*.

To mobilize a specific TDR from the bacterial chromosome, a functional pRel carrying two sgRNA spacers targeting the two ends of TDR is required to ensure accurate cleavage on the chromosome (Fig. 1B). Simultaneously, a functional pCap harboring a specific spacer–protospacer adjacent motif (PAM) cassette between the pair of homologous arms (HAs) is cleaved by sgRNA-Cas9, exposing the HAs, CapL, and CapR. The linearized pCap, the destination for BGC relocation, captures the mobilized TDR fragment through homologous recombination. Meanwhile, the Cas9-triggered double-strand break on the chromosome is repaired through homology-directed repair by HAs (DelL and DelR) cloned in the functional pRel. The relocated BGC on the multicopy plasmid undergoes replication

[1]Helmholtz Institute for Pharmaceutical Research Saarland (HIPS), Helmholtz Centre for Infection Research (HZI), Saarbrücken, Germany. [2]Helmholtz International Lab for Anti-Infectives, Helmholtz Centre for Infection Research, Braunschweig, Germany. [3]PharmaScienceHub, Saarbrücken, Germany. [4]Faculty of Medicine, Saarland University, Homburg, Germany. [5]Key Laboratory of South China Agricultural Plant Molecular Analysis and Genetic Improvement, South China Botanical Garden, Chinese Academy of Sciences, Guangzhou, China. [6]Department of Pharmacy, Saarland University, Saarbrücken, Germany. [7]German Center for Infection Research (DZIF), Braunschweig, Germany.
***Corresponding author. Email: rolf.mueller@helmholtz-hips.de (R.M.); chengzhang.fu@helmholtz-hips.de (C.F.)**
†These authors contributed equally to this work.

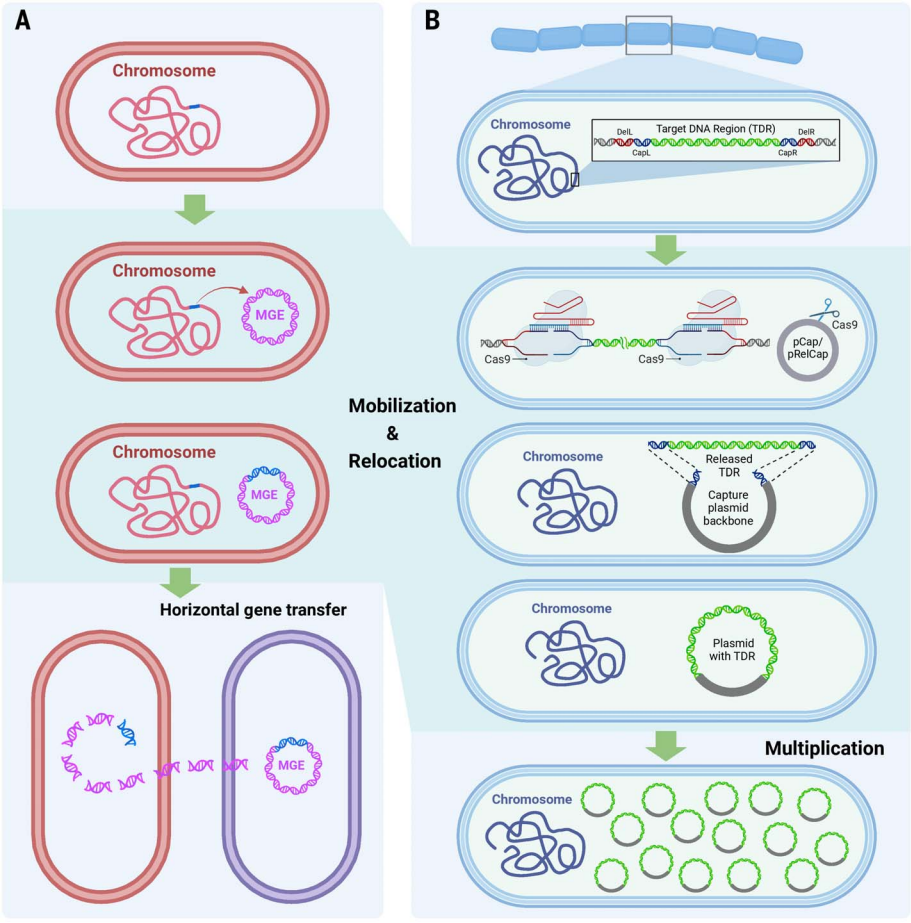

Fig. 1. The principle and design of ACTIMOT. (**A**) A representative spread model of antimicrobial resistance genes (ARGs, depicted in blue): (i) ARGs located on the bacterial chromosome are mobilized by either insertion sequences or integrons; (ii) the mobilized ARGs are transferred to mobile genetic elements (MGEs), such as plasmids; and (iii) the spread of ARGs is achieved through horizontal gene transfer. (**B**) Mobilization, relocation, and multiplication of target DNA regions (TDRs). The simulation of the transmission of ARGs involves the mobilization of TDRs in bacterial chromosomes through CRISPR-Cas9–mediated cuts. The relocation of released TDR into a cleaved multicopy plasmid and the repair of the chromosome are accomplished through homology-directed recombination. The TDR is then multiplied through the replication of the plasmid. [Figure created with BioRender.com]

dependent on the replicon of the pCap plasmid, potentially leading to the activation or enhancement of BGC expression through the gene dosage.

Proof of concept of ACTIMOT

To validate the concept of ACTIMOT, we selected the BGC of actinorhodins (*Act*), producing well-studied pigment compounds (*31*). Two working plasmids, namely pCap-101-Hyg-ACT-LR and pRel-ACT-dsp, were constructed (figs. S3 and S4) and introduced into *S. coelicolor* M145 through a two-step conjugation process. To examine the occurrence of the *Act* BGC mobilization from chromosome to plasmid, we isolated plasmids from 15 randomly picked M145 exconjugants. All samples showed the coverage of the two boundaries at the vector and the TDR sequence beyond the homologous arms through polymerase chain reaction (PCR) verification (fig. S5, A to C), suggesting the successful relocation of *Act* from the chromosome into the pCap plasmid within the cells.

To confirm the successful BGC relocation, we electroporated three PCR-verified plasmid samples into *E. coli* DH10B. Subsequent restriction digestion of the extracted plasmids revealed the correct presence of pCap-*Act*, harboring the 24-kb *Act* BGC, in four of the six randomly picked *E. coli* colonies (fig. S5, D and E). Furthermore, the successful recovery of pCap-*Act* depended on the presence of the functional pRel in the M145 strain, highlighting the crucial role of CRISPR-Cas9–mediated cleavage in the mobilization process (fig. S5F). The M145 exconjugants carrying the pCap-*Act* plasmid exhibited a darker color compared with the wild-type (WT) strain (Fig. 2B, upper panel, and fig. S6), indicating an enhanced production of the pigment actinorhodins in these mutants, likely due to the multiplication of the corresponding BGC. Moreover, the evident actinorhodin color observed in *S. lividans* ΔYA10 mutants expressing pCap-*Act* provides further support for the robustness and stability of ACTIMOT (Fig. 2B, lower panel). This proof-of-concept study demonstrates the feasibility of ACTIMOT and its potential to uncover hidden NPs from actinomycetes.

Discovery of NPs through improved single-plasmid ACTIMOT

Despite decades of exploration, the genus *Streptomyces* remains a prolific source of unknown BGCs (*11*, *12*, *15*, *32*). Conventional approaches, including activity-based random screening, have become less effective in discovering previously unidentified compounds. To address this challenge and explore the potential of ACTIMOT for uncovering uncharacterized NPs, we selected two type strains with reported compounds previously discovered by traditional methods, namely *S. avidinii* DSM40526 (*33*) and *S. armeniacus* DSM19369 (*34*, *35*).

The initial successful activation of the 24-kb *Act* prompted us to gradually increase the size of the TDRs in subsequent studies. The 48-kb TDR *Sav11* in the chromosome of *S. avidinii* DSM40526 appeared to be a promising candidate. It encompasses two adjacent unknown nonribosomal peptide synthetase (NRPS) BGCs, *avl* and *avs* (Fig. 3A, fig. S7, and table S5). The organization of the NRPS genes in a tail-to-tail manner and the presence of modular thioesterase domains indicate two separate BGCs. BGC *avs* comprises two NRPS genes with five modules, whereas BGC *avl* consists of multiple discrete NRPS and precursor biosynthesis genes. Further bioinformatic analyses indicated that both BGCs may yield uncharacterized compounds despite their broad distribution in different actinomycete strains (table S6 and data S1 to S4).

To mobilize *Sav11*, we constructed two functional plasmids, pCap-101-Apr-SAV11-LR and pRel-Hyg-SAV11-dsp, and then introduced them into *S. avidinii* using conjugation. PCR verification of the exconjugants confirmed the presence of the correct plasmid carrying the relocated *Sav11* (pCap-*Sav11*) (fig. S8A). As expected, upon transforming *E. coli* with plasmids extracted from verified *S. avidinii* exconjugants, we identified two colonies carrying the correct pCap-*Sav11* from 24 randomly selected transformants (fig. S8B). We further validated the completeness of the mobilized *Sav11* through short-read sequencing (fig. S9A). After meticulously examining the remaining 22 *E. coli* colonies, we identified the original empty pCap in every colony (fig. S8B). We hypothesized that the Cas9 protein expressed by pRel might not completely cleave the independent high-copy pCap

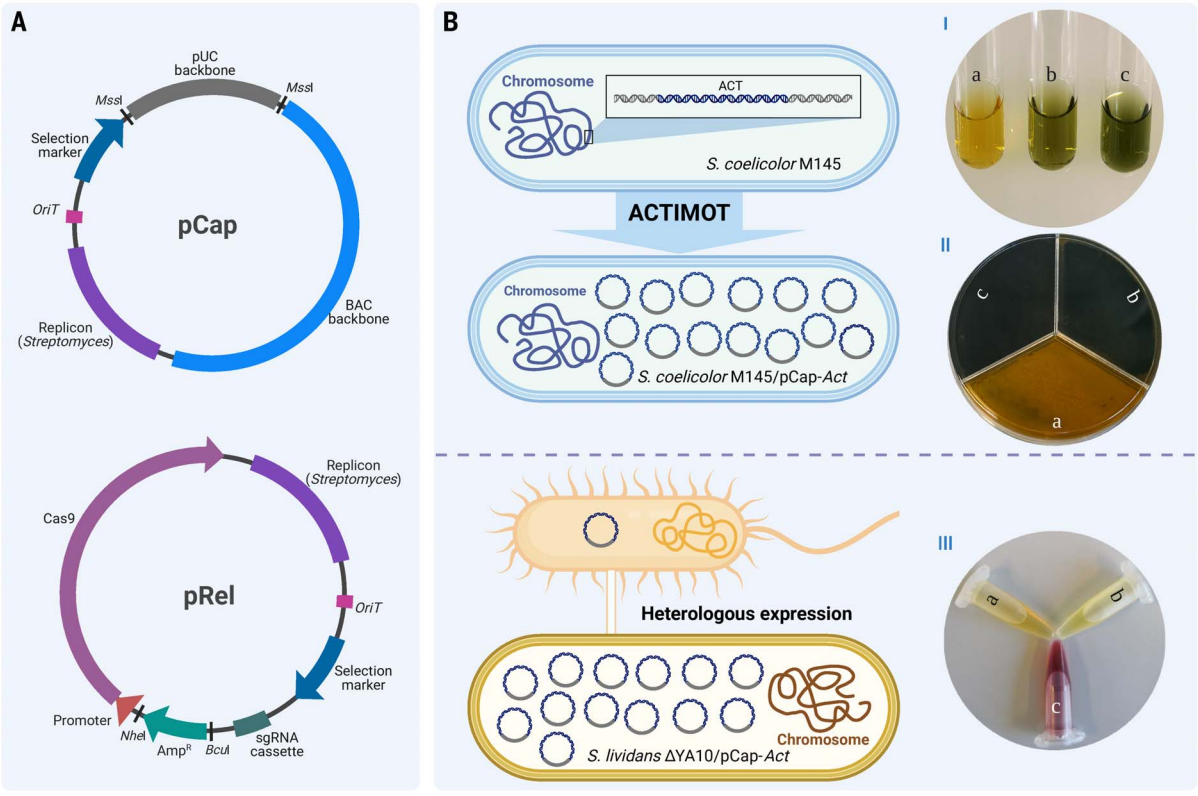

Fig. 2. The proof of concept of ACTIMOT. (**A**) Two sets of fundamental tool plasmids for ACTIMOT, pCap, and pRel. Detailed information about plasmid variants (different combinations of replicons and selection markers) is provided in fig. S1. (**B**) Production improvement of actinorhodin (ACT) by ACTIMOT in either native *Streptomyces coelicolor* M145 strain (up, I and II) or heterologous host (down, III). I (fermentation broth) and II (culture on agar plates) show *S. coelicolor* M145 WT (a) and two independent M145 mobilization mutants carrying pCap-*Act* [(b) and (c)]. III shows *S. lividans* ΔYA10 WT (a), ΔYA10 carrying empty pCap-Hyg-101-ACT-LR (b), and ΔYA10 carrying pCap-*Act* (c). [Figure partially created with BioRender.com]

in vivo, resulting in residual empty pCap in the mutants. To further improve the efficiency of ACTIMOT, we postulated that a CRISPR-Cas9–mediated self-cleavage could enhance the efficiency of cutting multicopy plasmids within cells. Therefore, we fused pCap-101-Apr-SAV11-LR and pRel-Hyg-SAV11-dsp (materials and methods), generating the single-plasmid pRelCap-SAV11-dsp for the mobilization of *Sav11*. Similarly to the dual-plasmid approach, we easily obtained and verified the correct exconjugants harboring the pCap-*Sav11* (fig. S8C). All *E. coli* colonies were confirmed to carry the correct pCap-*Sav11* after transformation with the plasmids extracted from *Streptomyces* exconjugants (fig. S8D), indicating improved efficiency of the single-plasmid ACTIMOT versus the dual-plasmid system for BGC mobilization (fig. S8E).

These two NRPS BGCs remained silent after the successful mobilization in *S. avidinii* because we did not detect prominent new compounds in chromatographic analysis in the correct mutants. We hypothesized that the expression of *Sav11* might still be repressed in the native host (*36*). Therefore, we transferred pCap-*Sav11* into the heterologous host *S. albus* Del14 (*37*) to escape the potential repression effect in the native strain, which led to the high-level production of dozens of compounds without any genetic modifications (Fig. 3, B, D, and E). We isolated the main compounds and structurally elucidated two types of peptides by nuclear magnetic resonance (NMR) and ultra-high-performance liquid chromatography–high-resolution mass spectrometry (UHPLC-HRMS) (figs. S10 to S13, S50 to S104, and tables S14 to S17). The stereochemistry of amino acid residues in these compounds was assigned by advanced Marfey's method (*38*) (figs. S14 to S17). Additionally, the structures of unisolated derivatives were elucidated through tandem MS (MS/MS) analysis (figs. S18 and S19).

We named the peptide families avidistatins (**1** to **7**) and avidilipopeptins (**8** to **22**) (Fig. 3, C and F, and fig. S19). Their corresponding BGCs were confirmed through gene deletion on the pCap-*Sav11* (fig. S20). Avidistatin A1 (**1**) is a linear acetylated pentapeptide composed of unusual nonproteogenic amino acid residues, including (2*S*,3*R*)-2,3-diamino-butyric acid [(2*S*,3*R*)-Dab] and (*Z*)-dehydrobutyrine (Dhb) (Fig. 3C). Avidistatin A2 (**2**) was identified as an isomer of **1**, on the basis of their identical molecular formulas and MS/MS data (fig. S18), whereas avidistatin B1 (**3**) and B2 (**4**) were characterized by the absence of the terminal serine residue present in **1**, as indicated by their MS/MS data (fig. S18). In avidistatins **5** to **7**, the 2,3-Dab residues were substituted with Dhb residues (Fig. 3C and fig. S18), which presumably undergo conversion through a C domain–mediated online dehydration from a threonyl residue (*39*). This observation suggests the potential promiscuity of the adenylation (A) domain within the second module (fig. S21). We confirmed the presence of (2*S*,3*R*)-Dab using the advanced Marfey's method (fig. S14). The genes *avsC*, *avsD*, and *avsE* are implicated in the formation of (2*S*,3*R*)-Dab because they show similarities to the previously reported (2*S*,3*R*)-Dab biosynthesis cassette (*40*). Recent studies have corroborated that analogous genes are responsible for the synthesis of (2*S*,3*R*)-Dab from threonine (*41*, *42*), supporting their roles in providing free substrate available for avidistatin assembly. Furthermore, the alignment of the majority of amino acid building blocks in avidistatin A with the A domain–specificity prediction in the *avs* pathway (table S7) strengthens the proposed biosynthetic pathway of avidistatins (fig. S21).

Avidilipopeptins are linear lipopeptides, including acylated pentapeptides **8** to **12**, **17** to **22**, and acylated dipeptides **13** to **16** (Fig. 3F).

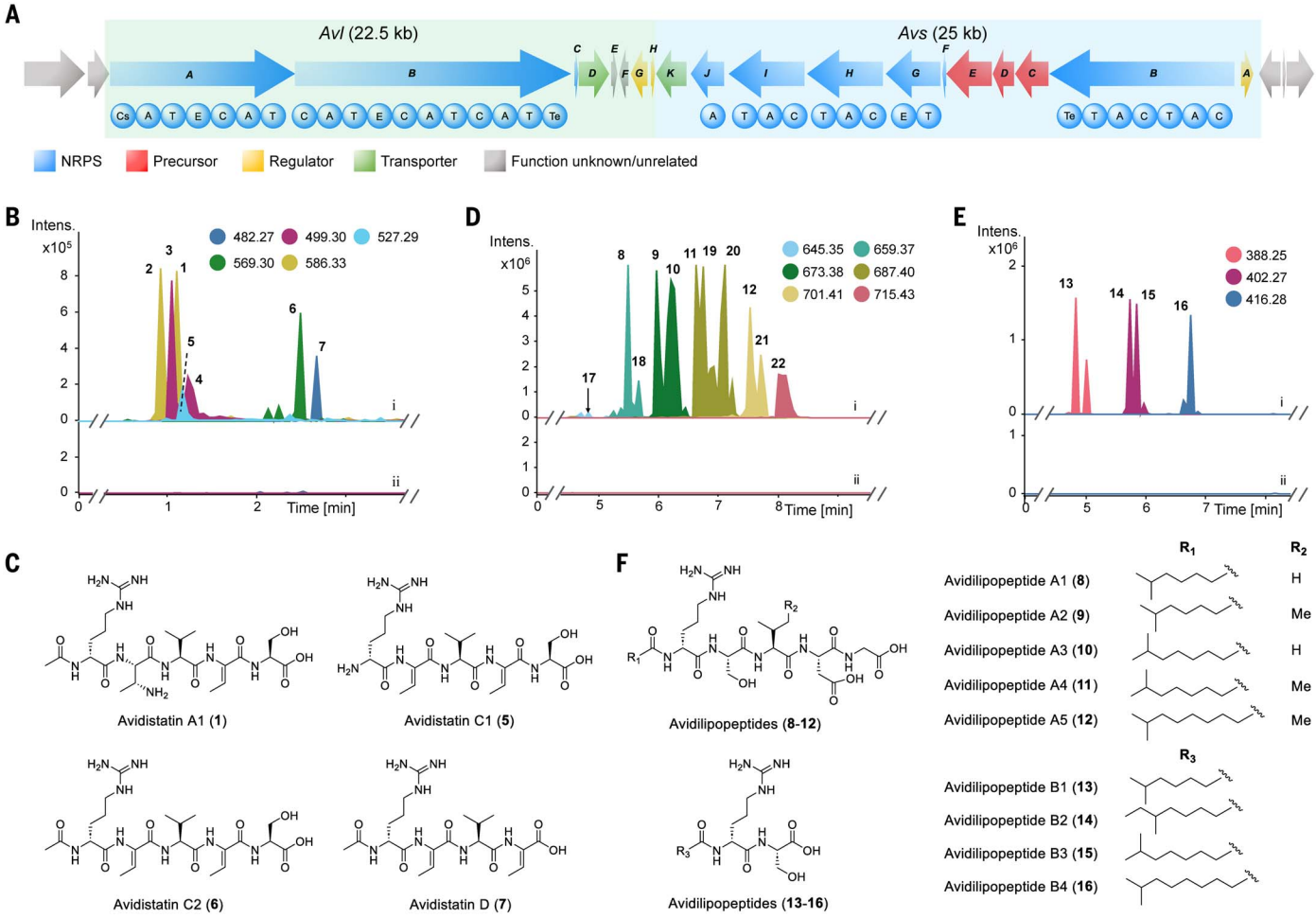

Fig. 3. Discovery of peptides by the improved single-plasmid ACTIMOT. (**A**) The organization of BGCs *avl* and *avs* in TDR *Sav11*. NRPS, nonribosomal peptide synthetase. (**B**) Extracted ion chromatograms (EICs) of avidistatins in crude extracts of *S. albus* Del14/pCap-*Sav11* (i) and *S. albus* Del14 (ii). The targeted mass/charge ratio (*m/z*) values are shown. (**C**) The structures of the identified avidistatins. (**D**) EICs of complete-length avidilipopeptins in crude extracts of *S. albus* Del14/pCap-*Sav11* (i) and *S. albus* Del14 (ii). The targeted *m/z* values are shown. (**E**) EICs of truncated avidilipopeptins in crude extracts of *S. albus* Del14/pCap-*Sav11* (i) and *S. albus* Del14 (ii). The targeted *m/z* values are shown. (**F**) The structures of the identified avidilipopeptins.

All characterized avidilipopeptins share the first two residues (D-arginine and L-serine), suggesting a potential pretermination step after the second NRPS module in the *avl* pathway (fig. S22). The diverse structures of avidistatins and avidilipopeptins highlight the strategies used by NRPS pathways to diversify the final products, including variable building blocks introduced by the promiscuous A domains and different chain lengths resulting from the optional chain release from the assembly line (figs. S21 and S22).

BGC multiplication facilitates the discovery of unusual lipopeptides

Building upon the success of the improved single-plasmid ACTIMOT, we expanded its application to activate other BGCs from different *Streptomyces* strains. Despite many BGCs present in the genome of *S. armeniacus* DSM19369, previous screening efforts by the pharmaceutical industry have only resulted in the discovery of armeniaspirols and streptopyrroles (*34*, *35*), underscoring the untapped biosynthetic potential to be explored by using different strategies. Among these, the 67-kb TDR *Sar13* emerged as a promising target, containing a cryptic "ladderane"-NRPS BGC *mop* (Fig. 4A, fig. S23, and table S8). The "ladderane"-NRPS BGCs are known to produce polyene-peptide hybrid compounds, such as ishigamide (*43*) and colibrimycins (*44*), or cinnamoyl-containing cyclodepsipeptides, such as kitacinnamycins (*45*) and skyllamycins (*46*, *47*). BGC *mop* shares more similarity with ishigamide BGC and colibrimycin BGCs than with those producing cinnamoyl-containing cyclodepsipeptides. ClusterBlast analysis (*48*) identified 34 similar BGCs distributed in various *Actinobacteria*, featuring a set of highly reducing type II polyketide synthase (PKS), NRPS modules, and 2,3-diaminopropionic acid (2,3-Dap) formation genes. These BGCs lack genes for benzene ring formation (*49*), deviating their products from cinnamoyl-containing compounds, which is corroborated by the linear polyene moieties present in ishigamide (*43*) and colibrimycins (*44*). These BGCs were categorized into various groups: 6 *mop* BGCs, 12 ishigamide BGCs, 4 colibrimycin BGCs, and 12 other unknown BGCs (table S10, and data S5 and S6), suggesting structural diversity encoded within this family. Exploring the products and biosynthesis of *mop* will deepen our knowledge of the structural features concealed within this BGC family.

To mobilize and activate *Sar13*, we constructed the plasmid pRelCap-SAR13-dsp and introduced it into *S. armeniacus*. Following the same validation procedure described in the *Sav11* mobilization, we verified the successful *Sar13* mobilization in 10 out of 11 plasmids derived from four randomly picked starting *Streptomyces* exconjugants (fig. S24), revealing a 90.9% success rate for *Sar13* mobilization. Short-read sequencing of pCap-*Sar13* further corroborated the integrity of the entire plasmid (fig. S9B).

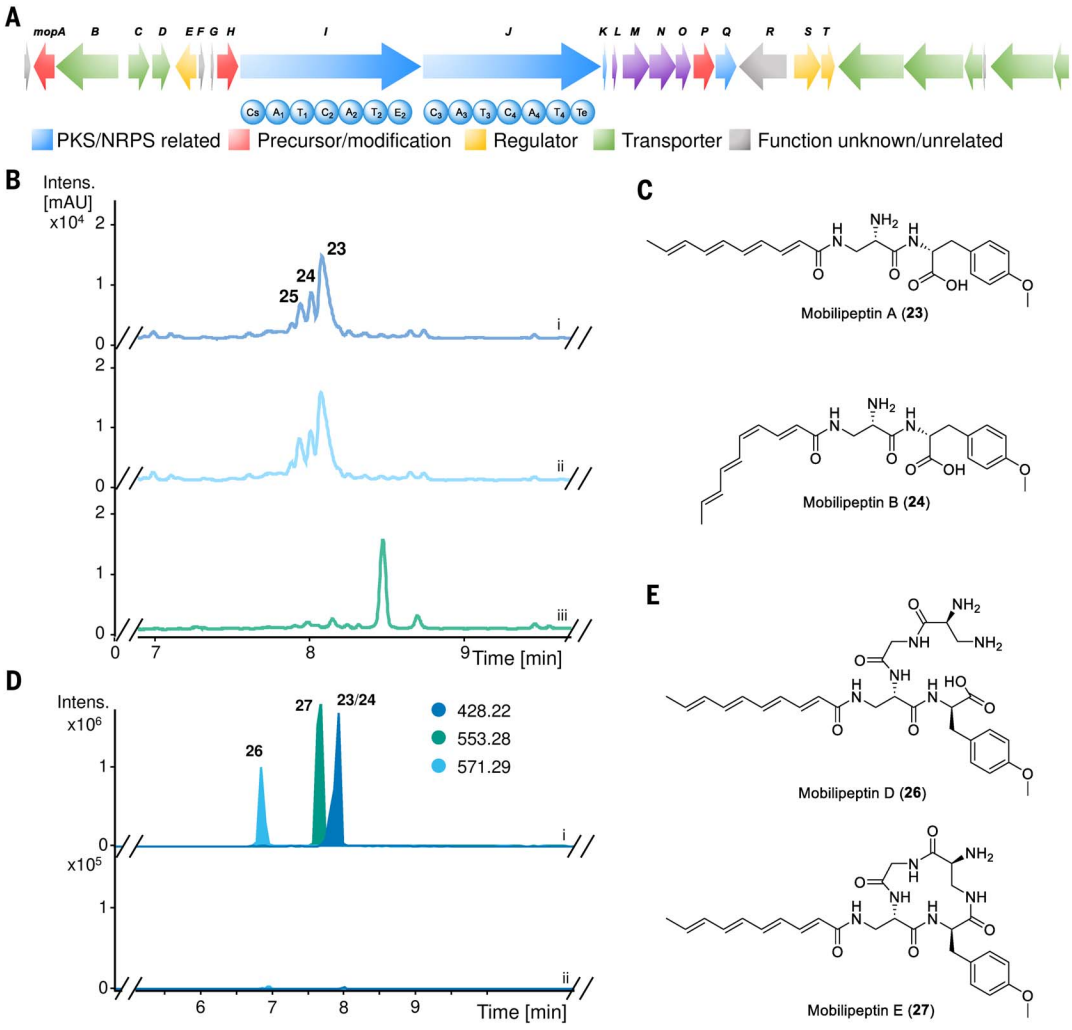

Fig. 4. The *mop* BGC multiplication unveils lipopeptides. (**A**) The organization of BGC *mop* in TDR *Sar13*. PKS, polyketide synthase. (**B**) Production enhancement of mobilipeptins through the mobilization and multiplication of *Sar13* in *S. armeniacus*. Chromatograms at ultraviolet wavelength of 336 nm are shown: (i) *S. armeniacus*/pCap-*Sar13* cultured in M2 medium plus 50 μg/ml apramycin, (ii) *S. armeniacus*/pCap-*Sar13* cultured in M2 medium without apramycin, and (iii) *S. armeniacus* cultured in M2 medium. (**C**) The structures of mobilipeptin A (**23**) and B (**24**). (**D**) Detection of mobilipeptins D (**26**), E (**27**), and A/B (**23**/**24**) in *S. armeniacus*/pCap-*Sar13* (i) and *S. albus* Del14/pCap-*Sar13*-int (ii). EICs are shown as depicted in the figure. The data presented in this panel are from the sampling with highest yield of **26** and **27** (day 2). (**E**) The structures of mobilipeptins D (**26**) and E (**27**).

The mobilization and multiplication of *Sar13* promoted the discovery of a series of metabolites that we named mobilipeptins. The yield of mobilipeptins in the mutants carrying mobilized *Sar13* increased nearly 40-fold (Fig. 4B and fig. S25). Discovering mobilipeptins directly from the WT of *S. armeniacus* would have been challenging because of their production in trace amounts that are only barely detectable with selective ion monitoring after the target mass is identified by using ACTIMOT (Fig. 4B and fig. S25A). The absence of selection antibiotics did not affect the production of mobilipeptins (Fig. 4B and fig. S25B), indicating the replication stability of the plasmid in the cells. This feature shows the potential of using ACTIMOT for increasing large-scale economic production of high-value NPs.

Structural elucidation by NMR, UHPLC-HRMS, and Marfey's method revealed that mobilipeptin A (**23**) and B (**24**) are lipopeptides containing a linear conjugated polyene chain coupled with a L-2,3-Dap and an *O*-methyl-D-tyrosine residue (Fig. 4C; figs. S26 to S28, S106 to S117; and table S18). The polyene chain is likely derived from the unusual type II PKS genes (*50*–*52*) present in the "ladderane" region of *Sar13*, whereas the dipeptide is installed by one of the NRPS genes with the starter condensation (Cs) domain (*mopI*). The substrates predicted for the two modules in MopI correspond closely with the observed residues (table S9). However, the sole TE domain in *mop* is situated after the glycine-recognizing NRPS module in MopJ (tables S8 and S9), hinting at the potential presence of precursor compounds with more residues present in the pathway. We hypothesized that this hybrid BGC initially produces precursor molecules with a tetrameric cyclic peptide core. This hypothesis is supported by the identification of an additional mobilipeptin congener **25**, featuring an extra glycine residue coupled to the α-amino group of L-2,3-Dap (fig. S29).

To explore the possibility of a structurally different primary product, we conducted fermentation under varying conditions. Numerous attempts resulted in the detection of short-lived products from the *Sar13*-activated mutant with corresponding molecular ions of $[M+H]^+$ = 571.29 (**26**, mobilipeptin D) and 553.28 (**27**, mobilipeptin E) at retention times of 6.7 and 7.5 min, respectively (Fig. 4D and fig. S30). These "transient" compounds exhibited their highest yield on day 2 when cultured in ISP4 medium but faded quickly in the subsequent fermentation (fig. S30). We next purified the tetracyclic peptide **27** from a 2-day fermentation of the *Sar13* mobilized mutant in ISP4. However, **27** exhibits extremely poor solubility in various solvents, including methanol, water, chloroform, and dimethyl sulfoxide, making the NMR measurement and the ensuing bioactivity test challenging. Unexpectedly, we found that **27** exhibited the desired solubility in acetone; however, the MS analysis of the solution showed **27** to convert to a new derivative **28** (fig. S31). Subsequently, we solved the structure of **28** through HRMS and NMR (figs. S26, S32, S118 to S123, and table S19), which suggested that **28** is an acetone adduct of **27**, which itself most likely exhibits a structure in line with the in silico prediction of substrate specificity of all the four A domains in *mop* (table S9). The deduced structure of **27** is a linear polyene chain coupled with tetracyclic peptide comprising

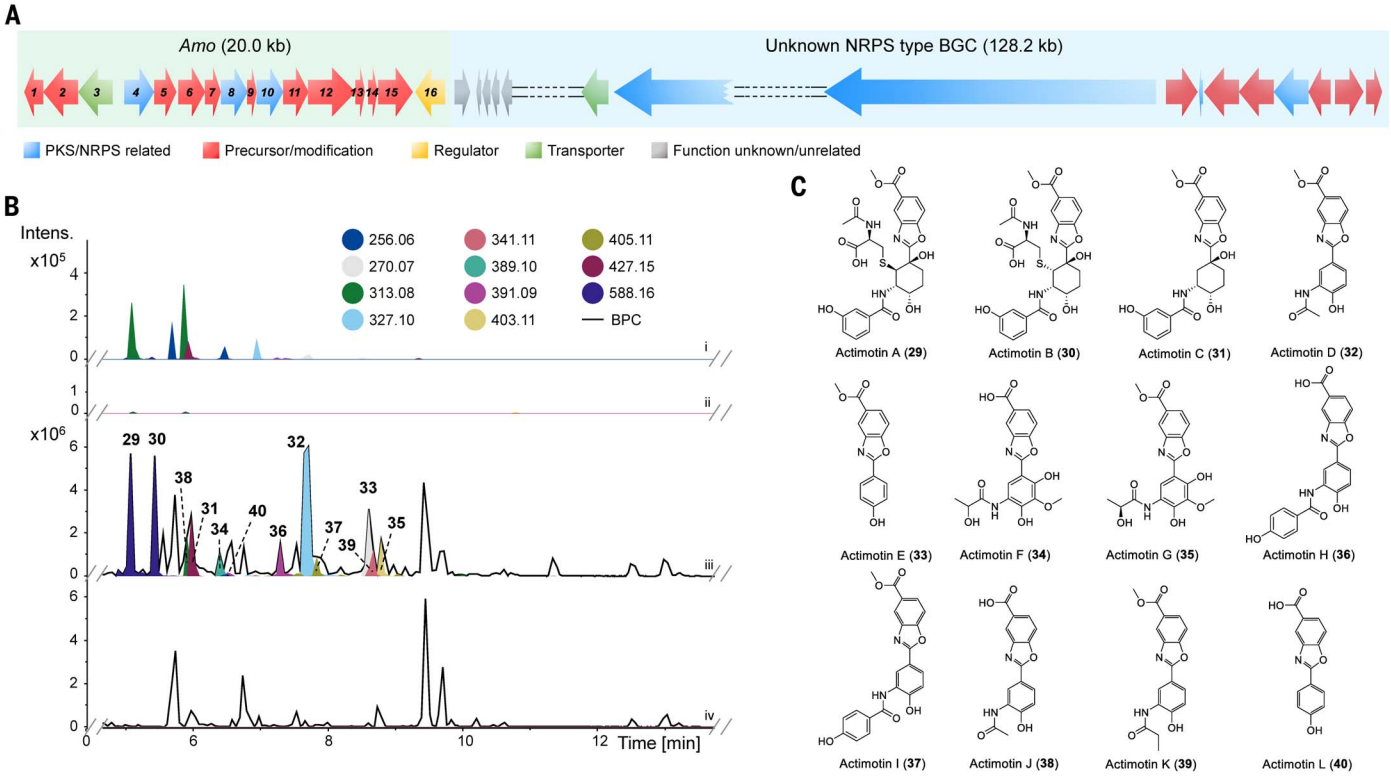

Fig. 5. Biosynthetic "dark matter" uncovered by ACTIMOT. (**A**) The scheme of the organization of TDR *Sav17*. (**B**) The activation of actimotins through ACTIMOT. EICs of representative actimotins in crude extracts of *S. avidinii*/pCap-*Sav17* (i), *S. avidinii* (ii), *S. albus* Del14/pCap-*Sav17* (iii), and *S. albus* Del14 (iv). The base peak chromatograms (BPCs) are also shown in traces iii and iv. (**C**) The structures of the identified actimotins.

two L-2,3-Dap residues, an *O*-methyl-D-tyrosine residue, and a glycine residue (Fig. 4E). Moreover, the structure of **26** was determined by MS fragmentation to be a degradation product of **27**, resulting from the hydrolysis of the amide bond between *O*-methyl-D-tyrosine and the third residue (L-2,3-Dap) (fig. S29), further supporting the structure assignment of **27**. Hence, we propose that **27** is the direct product released and cyclized from the NRPS of *mop*, which can be hydrolyzed into **26**, followed by stepwise cleavage into **23** to **25** (fig. S34).

Although direct degradation of **27** remains a plausible scenario, the identification of specific intermediates with different numbers of amino acid residues suggests that the tetracyclic peptide precursor could also undergo stepwise degradation by an as-yet-unknown mechanism (fig. S34). This process could involve rare enzyme-mediated cleavage, similar to that observed in the biosynthetic pathways of other peptides (*53*–*55*). The discovery of the cyclic mobilipeptin and a series of processing products of mobilipeptins has not only identified the likely authentic products of the *mop* pathway but also shed light on the biosynthesis and potential degradation mechanisms of mobilipeptins. Furthermore, the mobilipeptin biosynthetic pathway implies that the biosynthesis of ishigamide might also involve a cryptic cyclic peptide precursor. The direct activation of *mop* by ACTIMOT significantly enhanced the yield of mobilipeptins at different biosynthesis stages (Fig. 4D), which exemplified the distinctive capability of ACTIMOT.

Biosynthetic "dark matter" revealed by ACTIMOT

In our pursuit to uncover hidden biosynthetic potential, we embarked on mobilizing the colossal TDR *Sav17* from the chromosome of *S. avidinii* DSM40526. This expansive segment encompasses a massive 149-kb region predicted to harbor a giant NRPS BGC (Fig. 5A). This BGC comprises 28 NRPS modules with a Cs domain in the initial module, suggesting the potential production of large lipopeptides (fig. S35). A thorough ClusterBlast search on this BGC revealed a lack of similar BGCs within the current public database (data S7 and S8). After the mobilization procedure using the plasmid pRelCap-SAV17-dsp targeting the two ends of *Sav17* on the chromosome (fig. S36), we evaluated four exconjugants for the TDR mobilization efficiency. Subsequently, five out of eight random *E. coli* colonies obtained by transforming plasmids from the starting four *S. avidinii* exconjugants were found to harbor the plasmid pCap-*Sav17* that contains the correct 149-kb DNA region (fig. S37). Further short-read sequencing of the plasmids confirmed the integrity of the mobilized *Sav17*, suggesting the high fidelity of ACTIMOT (fig. S9C). In the *S. avidinii* mutants carrying pCap-*Sav17*, we identified a series of highly yield-improved compounds that were easy to neglect in the WT strain because of their meager production (Fig. 5B). This observation indicated the activation of a cryptic BGC within *Sav17*. Subsequently, the heterologous expression of pCap-*Sav17* in *S. albus* Del14 showed a much higher production of the compounds found in *S. avidinii* and multiple new compounds (Fig. 5B). Through comprehensive analysis using NMR and UHPLC-HRMS/MS, we purified and structurally elucidated nine compounds (**29** to **36**, and **38**), unveiling a family of benzoxazole-containing compounds that we named actimotins (Fig. 5C; figs. S38 to S40, S124 to S176; and tables S20 to S23). The stereochemical configurations of **31** and **35** were determined with Mosher ester analysis (fig. S39 and tables S24 and S25), and the stereochemistry of **29** and **30** was assigned through density-functional theory simulation (figs. S41 to S45). MS/MS analysis facilitated the identification of the structures of three additional derivatives (**37**, **39**, and **40**) (fig. S46). One notable structural feature of actimotins, alongside their rare metasubstituted benzoxazole pattern, is the (1*S*,2*R*,4*S*)-2-aminocyclohexane-1,4-diol (ACHD) moiety in several congeners (**29** to **31**).

We did not find the reported benzoxazole BGC in *sav17* (*56*). The only plausible candidate

is an upstream 20-kb region enriched with various biosynthetic genes, including discrete A domain genes, which we initially presumed to be part of the giant NRPS BGC. Through gene deletions and heterologous expression of the modified *sav17* (Fig. 5A, fig. S47, and table S11), we confirmed that this cryptic 16-gene region is responsible for actimotin biosynthesis, distinct from the giant NRPS BGC. Thus, ACTIMOT paved the way for discovering the actimotin biosynthetic pathway, which was not identified by in silico prediction owing to the limited understanding of the biosynthesis of metasubstituted benzoxazoles. During our study on actimotin biosynthesis, the first BGC encoding for metasubstituted benzoxazoles was published (*57*). However, genome mining efforts by these authors using the respective BGC did not provide any hint at the actimotin pathway (*57*), probably because of low sequence similarity (table S12). Even the recently updated antiSMASH (v7.0) did not predict the actimotin pathway, further confirming its distinctiveness.

Amo5 shows 38.9% amino acid identity to GriI, and Amo6 exhibits 39.1% identity to GriH from the grixazone BGC. GriI and GriH have been shown to be responsible for the biosynthesis of 3-amino-4-hydroxybenzoic acid (3,4-AHBA) from L-aspartate-4-semialdehyde and dihydroxyacetone phosphate (*58*), and we suggest that Amo5 and Amo6 play similar roles in 3,4-AHBA formation in actimotin biosynthesis. The BGC *amo* encodes three phenylacetate-CoA ligase family proteins—Amo4, Amo8, and Amo10—which exhibit low sequence identities to ClxA and ClxC (table S12), implying their involvement in activating and linking residues in the actimotin biosynthetic pathway. The amidohydrolase Amo7, which is homologous to ClxD, likely catalyzes the formation of the oxazole moiety through heterocyclization. In actimotin derivatives featuring a third benzoyl residue (**29** to **31**, **36**, and **37**), this residue is attached to the 3-amino group of the benzoxazole scaffold (Fig. 5C). This linkage pattern differs from the one observed in closoxazoles (*57*), suggesting the absence of a ClxC-like ligase in *amo*. Furthermore, actimotins exhibit additional structural diversity, primarily arising from the variation of the second and the third residues (Fig. 5C and fig. S49). The promiscuity of corresponding phenylacetate-CoA ligases likely explains these variations.

To investigate whether the ACHD moiety shares the same biosynthetic origin with 3,4-AHBA, we conducted a feeding experiment using isotope-labeled L-aspartic acid-$^{13}C_4$,^{15}N on the mutant carrying pCap-*Sav17*. Because L-aspartate-4-semialdehyde is derived from L-aspartate (*59*), this approach allowed us to trace the incorporation of the labeled precursor. Our results indicated a double incorporation of the labeled precursor skeleton in actimotin J (**38**) and D (**32**) (fig. S48, A and B), both of which contain two 3,4-AHBA units (Fig. 5C). The incorporation rate was low (fig. S48, A and B), which likely results from the use of aspartic acid in primary metabolism and additional catalytic steps required before incorporation into actimotin (*59*). A similarly low incorporation rate was observed in actimotin A (**29**) and B (**30**) (fig. S48, C and D), suggesting that the ACHD moiety originates from 3,4-AHBA through stepwise reductions, although alternative pathways cannot be excluded. Further feeding with L-cysteine-$^{13}C_3$,^{15}N revealed a 4 Da difference between control and isotope-labeled **29** and **30** (fig. S48, E and F), indicating that L-cysteine serves as the precursor for their *N*-acetylcysteinyl moieties. A previous study on grixazole biosynthesis showed that *N*-acetylcysteine (NAC) nonenzymatically links to an *o*-quinone imine derivative, oxidized from 3-amino-4-hydroxybenzaldehyde by a tyrosinase-like enzyme, GriF (*60*). Although *amo* lacks a GriF-like oxidase, we hypothesize that NAC incorporation into the actimotin pathway might be facilitated by a different oxidoreductase, leading to the production of **29** and **30** (fig. S49). The structural diversity among actimotins suggests the involvement of various tailoring genes that modify the core benzoxazole structure, warranting further investigation (fig. S49).

We subsequently conducted a comprehensive survey to explore the distribution of *amo*-like BGCs featuring analogous genes to *amo5*, *amo6*, *amo7*, and *amo4*/*amo8*, which are core benzoxazole biosynthetic genes. Among the 383 hits harboring all the four essential genes uncovered, 364 were identified as full-length BGCs and the remaining 19 were fragmented because of sequence quality issues (data S9). These 364 BGCs include two actimotin BGCs and 45 closoxazole BGCs (*clx*), along with two BGCs analogous to *amo* and 35 BGCs similar to *clx*. The remaining 280 BGCs, each containing one to four phenylacetate-CoA ligases, diverge from both known categories. This variety indicates a potential structural diversity of *amo*-like BGC products in nature.

Lastly, in our exploration of the bioactivity of the four compound classes obtained in this work, only actimotin G (**35**) exhibited weak activity toward *E. coli* Δ*tolC*, whereas all other compounds showed no appreciable bioactivity against different microorganisms and a human cell line (table S13).We noticed that the actimotins share the benzoxazole structural feature with tafamidis, a drug used medicinally as a transthyretin (TTR) stabilizer to treat TTR amyloidosis-related diseases (*61*, *62*). TTR is a homotetramic transport protein in human plasma responsible for transporting thyroxine (T_4) and retinol (*63*). TTR amyloid fibrils are associated with various diseases, including familial amyloidotic polyneuropathy (FAP) (*64*) and familial amyloid cardiomyopathy (FAC) (*65*). The TTR mutant V30M (TTR-V30M) is the most common variant linked to TTR amyloidosis (*66*). To evaluate a potential similar activity of actimotins, we developed a thioflavin T-based assay to stabilize the TTR-V30M, on the basis of a previous study (*67*). In our assays with 10 μM TTR-V30M, tafamidis, used as positive control, showed activity with a median effective concentration (EC_{50}) value of 9.8 μM (fig. S50A), which is consistent with the previous report (*68*). Among the isolated actimotins, actimotin J (**38**) exhibited activity in a similar range, with an EC_{50} value of 67.8 μM (fig. S50B). Actimotin J shares the same structure with a previously isolated metasubstituted benzoxazole from *Nocardiopsis lucentensis* DSM44048, which was also reported to show no cell-based bioactivity (*69*). Our finding holds promise for discovering further actimotin derivatives exhibiting TTR amyloidogenesis inhibition activity from the identified *amo*-like BGCs. The observation of the TTR-stabilizing activity of actimotin J implies that these compounds warrant further evaluation in various assays, particularly non–cell based assays, to better understand their potential and biological function.

Conclusions

As a technological advancement, ACTIMOT integrates BGC cloning and activation stages through one-step manipulation–triggered mobilization, relocation, and multiplication within native bacterial strains. This approach streamlines the process, requiring only a few basic cloning steps for small DNA fragments in *E. coli*. It holds the potential to directly enhance compound yields from target BGCs without excessive manipulation. ACTIMOT outperforms a cloning-independent approach that uses integrase-triggered site-specific recombination in native bacterial cells (*70*), which is hampered by the complexity of three-step conjugations and the tedious screening required at each step. ACTIMOT's efficiency and simplicity make it a promising candidate for integration with other approaches, such as BGC engineering through promoter refactoring and heterologous expression in suitable hosts. Recent studies (*71*, *72*) have introduced intriguing BGC expression strategies, with a landing pad (LP)–mediated bacteria domestication method playing an important role in host domestication and efficient BGC expression. These LP-based domestication-expression frameworks present opportunities to enhance the versatility of ACTIMOT. Our research underscores ACTIMOT's prowess by unearthing four previously unknown compound categories without altering the native BGCs. Particularly noteworthy is the unexpected identification of actimotins, whose BGC defies prediction by current in silico tools, hinting at ACTIMOT's potential for uncovering unpredictable pathways in future investigations. Additionally, the identification of the hidden cyclic mobilipeptin precursor demonstrates the

power of ACTIMOT in boosting NP discovery. The achievements of ACTIMOT in *Streptomyces* fuel optimism about its potential applicability in rare actinomycetes, owing to compatible replicons (*73*). Although the current application range of ACTIMOT is limited and depends on the genetic tractability of target strains, it shows potential in other genetically manipulable and BGC-rich bacterial species, such as *Proteobacteria* and *Firmicutes* (*11*). To broaden its utility, further efforts are needed to develop compatible genetic elements, thereby expanding the scope of ACTIMOT's applicability. These future applications will allow for a more comprehensive assessment of its broader impacts. In summary, this study demonstrates the potential of ACTIMOT as a strategy to discover previously unkown NPs across diverse microorganisms. ACTIMOT stands poised to unlock the vast genomic potential within these NP factories and to expand known biochemical space.

Methods summary

A detailed description of the methods, including plasmid design and production, BGC mobilization, bioinformatics analysis, bacterial growth conditions, natural product isolation and characterization, and biological activity testing, can be found in the supplementary materials.

REFERENCES AND NOTES

1. World Health Organization, "Antimicrobial resistance," 21 November 2023; https://www.who.int/news-room/fact-sheets/detail/antimicrobial-resistance.
2. D. G. J. Larsson, C.-F. Flach, Antibiotic resistance in the environment. *Nat. Rev. Microbiol.* **20**, 257–269 (2022). doi: 10.1038/s41579-021-00649-x; pmid: 34737424
3. M. A. Cook, G. D. Wright, The past, present, and future of antibiotics. *Sci. Transl. Med.* **14**, eabo7793 (2022). doi: 10.1126/scitranslmed.abo7793; pmid: 35947678
4. M. Razavi, E. Kristiansson, C.-F. Flach, D. G. J. Larsson, The association between insertion sequences and antibiotic resistance genes. *MSphere* **5**, e00418-20 (2020). doi: 10.1128/mSphere.00418-20; pmid: 32878926
5. Y. Che *et al*., Conjugative plasmids interact with insertion sequences to shape the horizontal transfer of antimicrobial resistance genes. *Proc. Natl. Acad. Sci. U.S.A.* **118**, e2008731118 (2021). doi: 10.1073/pnas.2008731118; pmid: 33526659
6. M. Gillings *et al*., The evolution of class 1 integrons and the rise of antibiotic resistance. *J. Bacteriol.* **190**, 5095–5100 (2008). doi: 10.1128/JB.00152-08; pmid: 18487337
7. M. Razavi *et al*., Discovery of the fourth mobile sulfonamide resistance gene. *Microbiome* **5**, 160 (2017). doi: 10.1186/s40168-017-0379-y; pmid: 29246178
8. S. Castañeda-Barba, E. M. Top, T. Stalder, Plasmids, a molecular cornerstone of antimicrobial resistance in the One Health era. *Nat. Rev. Microbiol.* **22**, 18–32 (2024). doi: 10.1038/s41579-023-00926-x; pmid: 37430173
9. D. J. Newman, G. M. Cragg, Natural products as sources of new drugs over the nearly four decades from 01/1981 to 09/2019. *J. Nat. Prod.* **83**, 770–803 (2020). doi: 10.1021/acs.jnatprod.9b01285; pmid: 32162523
10. K. Lewis, The science of antibiotic discovery. *Cell* **181**, 29–45 (2020). doi: 10.1016/j.cell.2020.02.056; pmid: 32197064
11. A. Gavriilidou *et al*., Compendium of specialized metabolite biosynthetic diversity encoded in bacterial genomes. *Nat. Microbiol.* **7**, 726–735 (2022). doi: 10.1038/s41564-022-01110-2; pmid: 35505244
12. F. Hemmerling, J. Piel, Strategies to access biosynthetic novelty in bacterial genomes for drug discovery. *Nat. Rev. Drug Discov.* **21**, 359–378 (2022). doi: 10.1038/s41573-022-00414-6; pmid: 35296832
13. L. Huo *et al*., Heterologous expression of bacterial natural product biosynthetic pathways. *Nat. Prod. Rep.* **36**, 1412–1436 (2019). doi: 10.1039/C8NP00091C; pmid: 30620035
14. K. Scherlach, C. Hertweck, Mining and unearthing hidden biosynthetic potential. *Nat. Commun.* **12**, 3864 (2021). doi: 10.1038/s41467-021-24133-5; pmid: 34162873
15. A. G. Atanasov, S. B. Zotchev, V. M. Dirsch, C. T. Supuran, International Natural Product Sciences Taskforce, Natural products in drug discovery: Advances and opportunities. *Nat. Rev. Drug Discov.* **20**, 200–216 (2021). doi: 10.1038/s41573-020-00114-z; pmid: 33510482
16. F. Panter, C. D. Bader, R. Müller, Synergizing the potential of bacterial genomics and metabolomics to find novel antibiotics. *Chem. Sci.* **12**, 5994–6010 (2021). doi: 10.1039/D0SC06919A; pmid: 33995996
17. A. Bauermeister, H. Mannochio-Russo, L. V. Costa-Lotufo, A. K. Jarmusch, P. C. Dorrestein, Mass spectrometry-based metabolomics in microbiome investigations. *Nat. Rev. Microbiol.* **20**, 143–160 (2022). doi: 10.1038/s41579-021-00621-9; pmid: 34552265
18. M. H. Medema, T. de Rond, B. S. Moore, Mining genomes to illuminate the specialized chemistry of life. *Nat. Rev. Genet.* **22**, 553–571 (2021). doi: 10.1038/s41576-021-00363-7; pmid: 34083778
19. A. F. Rosenzweig, J. Burian, S. F. Brady, Present and future outlooks on environmental DNA-based methods for antibiotic discovery. *Curr. Opin. Microbiol.* **75**, 102335 (2023). doi: 10.1016/j.mib.2023.102335; pmid: 37327680
20. B. C. Covington, F. Xu, M. R. Seyedsayamdost, A natural product chemist's guide to unlocking silent biosynthetic clusters. *Annu. Rev. Biochem.* **90**, 763–788 (2021). doi: 10.1146/annurev-biochem-081420-102432; pmid: 33848426
21. M. Miethke *et al*., Towards the sustainable discovery and development of new antibiotics. *Nat. Rev. Chem.* **5**, 726–749 (2021). doi: 10.1038/s41570-021-00313-1
22. R. H. Baltz, Natural product drug discovery in the genomic era: Realities, conjectures, misconceptions, and opportunities. *J. Ind. Microbiol. Biotechnol.* **46**, 281–299 (2019). doi: 10.1007/s10295-018-2115-4; pmid: 30484124
23. M. Jinek *et al*., A programmable dual-RNA-guided DNA endonuclease in adaptive bacterial immunity. *Science* **337**, 816–821 (2012). doi: 10.1126/science.1225829; pmid: 22745249
24. L. Cong *et al*., Multiplex genome engineering using CRISPR/Cas systems. *Science* **339**, 819–823 (2013). doi: 10.1126/science.1231143; pmid: 23287718
25. P. Mali *et al*., RNA-guided human genome engineering via Cas9. *Science* **339**, 823–826 (2013). doi: 10.1126/science.1232033; pmid: 23287722
26. R. E. Cobb, Y. Wang, H. Zhao, High-efficiency multiplex genome editing of *Streptomyces* species using an engineered CRISPR/Cas system. *ACS Synth. Biol.* **4**, 723–728 (2015). doi: 10.1021/sb500351f; pmid: 25458909
27. Y. Tong, P. Charusanti, L. Zhang, T. Weber, S. Y. Lee, CRISPR-Cas9 based engineering of actinomycetal genomes. *ACS Synth. Biol.* **4**, 1020–1029 (2015). doi: 10.1021/acssynbio.5b00038; pmid: 25806970
28. L. Sandegren, D. I. Andersson, Bacterial gene amplification: Implications for the evolution of antibiotic resistance. *Nat. Rev. Microbiol.* **7**, 578–588 (2009). doi: 10.1038/nrmicro2174; pmid: 19609259
29. G. Muth, W. Wohlleben, A. Pühler, The minimal replicon of the *Streptomyces ghanaensis* plasmid pSG5 identified by subcloning and Tn5 mutagenesis. *Mol. Gen. Genet.* **211**, 424–429 (1988). doi: 10.1007/BF00425695; pmid: 18297777
30. Z. X. Deng, T. Kieser, D. A. Hopwood, "Strong incompatibility" between derivatives of the *Streptomyces* multi-copy plasmid pIJ101. *Mol. Gen. Genet.* **214**, 286–294 (1988). doi: 10.1007/BF00337723; pmid: 3070352
31. S. Okamoto, T. Taguchi, K. Ochi, K. Ichinose, Biosynthesis of actinorhodin and related antibiotics: Discovery of alternative routes for quinone formation encoded in the *act* gene cluster. *Chem. Biol.* **16**, 226–236 (2009). doi: 10.1016/j.chembiol.2009.01.015; pmid: 19246012
32. O. Genilloud, Actinomycetes: Still a source of novel antibiotics. *Nat. Prod. Rep.* **34**, 1203–1232 (2017). doi: 10.1039/C7NP00026J; pmid: 28820533
33. E. O. Stapley, J. M. Mata, I. M. Miller, T. C. Demny, H. B. Woodruff, Antibiotic MSD-235. I. Production by *Streptomyces avidinii* and *Streptomyces lavendulae*. *Antimicrob. Agents Chemother.* **161**, 20–27 (1963). pmid: 14274896
34. C. Dufour *et al*., Isolation and structural elucidation of armeniaspirols A-C: Potent antibiotics against gram-positive pathogens. *Chemistry* **18**, 16123–16128 (2012). doi: 10.1002/chem.201201635; pmid: 23143837
35. C. Fu *et al*., Armeniaspirol antibiotic biosynthesis: Chlorination and oxidative dechlorination steps affording spiro4.4non-8-ene. *ChemBioChem* **20**, 764–769 (2019). doi: 10.1002/cbic.201800791; pmid: 30556942
36. B. Aigle, C. Corre, Waking up *Streptomyces* secondary metabolism by constitutive expression of activators or genetic disruption of repressors. *Methods Enzymol.* **517**, 343–366 (2012). doi: 10.1016/B978-0-12-404634-4.00017-6; pmid: 23084947
37. M. Myronovskyi *et al*., Generation of a cluster-free *Streptomyces albus* chassis strains for improved heterologous expression of secondary metabolite clusters. *Metab. Eng.* **49**, 316–324 (2018). doi: 10.1016/j.ymben.2018.09.004; pmid: 30196100
38. P. Marfey, Determination of D-amino acids. II. Use of a bifunctional reagent, 1,5-difluoro-2,4-dinitrobenzene. *Carlsberg Res. Commun.* **49**, 591–596 (1984). doi: 10.1007/BF02908688
39. S. Wang *et al*., Discovery and biosynthetic investigation of a new antibacterial dehydrated non-ribosomal tripeptide. *Angew. Chem. Int. Ed.* **60**, 3229–3237 (2021). doi: 10.1002/anie.202012902; pmid: 33107670
40. C. Müller *et al*., Sequencing and analysis of the biosynthetic gene cluster of the lipopeptide antibiotic Friulimicin in *Actinoplanes friuliensis*. *Antimicrob. Agents Chemother.* **51**, 1028–1037 (2007). doi: 10.1128/AAC.00942-06; pmid: 17220414
41. R. Li, M. S. Lichstrahl, T. A. Zandi, L. Kahlert, C. A. Townsend, The *dabABC* operon is a marker of C4-alkylated monobactam biosynthesis and responsible for (*2S*,*3R*)-diaminobutyrate production. *iScience* **27**, 109202 (2024). doi: 10.1016/j.isci.2024.109202; pmid: 38433893
42. S. Sakata *et al*., Identification of the cirratiomycin biosynthesis gene cluster in *Streptomyces cirratus*: Elucidation of the biosynthetic pathways for 2,3-diaminobutyric acid and hydroxymethylserine. *Chemistry* **30**, e202400271 (2024). doi: 10.1002/chem.202400271; pmid: 38456538
43. D. Du *et al*., Production of a novel amide-containing polyene by activating a cryptic biosynthetic gene cluster in *Streptomyces* sp. MSC090213JE08. *ChemBioChem* **17**, 1464–1471 (2016). doi: 10.1002/cbic.201600167; pmid: 27311327
44. L. Prado-Alonso *et al*., Colibrimycins, novel halogenated hybrid polyketide synthase-nonribosomal peptide synthetase (PKS-NRPS) compounds produced by *Streptomyces* sp. strain CS147. *Appl. Environ. Microbiol.* **88**, e0183921 (2022). doi: 10.1128/AEM.01839-21; pmid: 34669429
45. J. Shi *et al*., Genome mining and biosynthesis of kitacinnamycins as a STING activator. *Chem. Sci.* **10**, 4839–4846 (2019). doi: 10.1039/C9SC00815B; pmid: 31160959
46. J. Bracegirdle *et al*., Skyllamycins D and E, non-ribosomal cyclic depsipeptides from lichen-sourced *Streptomyces anulatus*. *J. Nat. Prod.* **84**, 2536–2543 (2021). doi: 10.1021/acs.jnatprod.1c00547; pmid: 34490774
47. S. Pohle, C. Appelt, M. Roux, H.-P. Fiedler, R. D. Süssmuth, Biosynthetic gene cluster of the non-ribosomally synthesized cyclodepsipeptide skyllamycin: Deciphering unprecedented ways of unusual hydroxylation reactions. *J. Am. Chem. Soc.* **133**, 6194–6205 (2011). doi: 10.1021/ja108971p; pmid: 21456593
48. K. Blin *et al*., antiSMASH 7.0: New and improved predictions for detection, regulation, chemical structures and visualisation. *Nucleic Acids Res.* **51**, W46–W50 (2023). doi: 10.1093/nar/gkad344; pmid: 37140036
49. J. Shi *et al*., *In vitro* reconstitution of cinnamoyl moiety reveals two distinct cyclases for benzene ring formation. *J. Am. Chem. Soc.* **144**, 7939–7948 (2022). doi: 10.1021/jacs.2c02855; pmid: 35470672
50. D. Du, Y. Katsuyama, K. Shin-Ya, Y. Ohnishi, Reconstitution of a type II polyketide synthase that catalyzes polyene formation. *Angew. Chem. Int. Ed.* **57**, 1954–1957 (2018). doi: 10.1002/anie.201709636; pmid: 29265713
51. D. Du *et al*., Structural basis for selectivity in a highly reducing type II polyketide synthase. *Nat. Chem. Biol.* **16**, 776–782 (2020). doi: 10.1038/s41589-020-0530-0; pmid: 32367018
52. G. L. C. Grammbitter *et al*., An uncommon type II PKS catalyzes biosynthesis of aryl polyene pigments. *J. Am. Chem. Soc.* **141**, 16615–16623 (2019). doi: 10.1021/jacs.8b10776; pmid: 30908039
53. C. Fu *et al*., Biosynthetic studies of telomycin reveal new lipopeptides with enhanced activity. *J. Am. Chem. Soc.* **137**, 7692–7705 (2015). doi: 10.1021/jacs.5b01794; pmid: 26043159
54. J. Masschelein *et al*., A combination of polyunsaturated fatty acid, nonribosomal peptide and polyketide biosynthetic machinery is used to assemble the zeamine antibiotics. *Chem. Sci.* **6**, 923–929 (2015). doi: 10.1039/C4SC01927J; pmid: 29560178

55. Y.-M. Shi *et al*., Global analysis of biosynthetic gene clusters reveals conserved and unique natural products in entomopathogenic nematode-symbiotic bacteria. *Nat. Chem.* **14**, 701–712 (2022). doi: 10.1038/s41557-022-00923-2; pmid: 35469007
56. M. Lv, J. Zhao, Z. Deng, Y. Yu, Characterization of the biosynthetic gene cluster for benzoxazole antibiotics A33853 reveals unusual assembly logic. *Chem. Biol.* **22**, 1313–1324 (2015). doi: 10.1016/j.chembiol.2015.09.005; pmid: 26496684
57. T. Horch *et al*., Alternative benzoxazole assembly discovered in anaerobic bacteria provides access to privileged heterocyclic scaffold. *Angew. Chem. Int. Ed.* **61**, e202205409 (2022). doi: 10.1002/anie.202205409; pmid: 35656913
58. H. Suzuki, Y. Ohnishi, Y. Furusho, S. Sakuda, S. Horinouchi, Novel benzene ring biosynthesis from C(3) and C(4) primary metabolites by two enzymes. *J. Biol. Chem.* **281**, 36944–36951 (2006). doi: 10.1074/jbc.M608103200; pmid: 17003031
59. R. E. Viola, The central enzymes of the aspartate family of amino acid biosynthesis. *Acc. Chem. Res.* **34**, 339–349 (2001). doi: 10.1021/ar000057q; pmid: 11352712
60. H. Suzuki, Y. Furusho, T. Higashi, Y. Ohnishi, S. Horinouchi, A novel *o*-aminophenol oxidase responsible for formation of the phenoxazinone chromophore of grixazone. *J. Biol. Chem.* **281**, 824–833 (2006). doi: 10.1074/jbc.M505806200; pmid: 16282322
61. T. Coelho *et al*., Long-term effects of tafamidis for the treatment of transthyretin familial amyloid polyneuropathy. *J. Neurol.* **260**, 2802–2814 (2013). doi: 10.1007/s00415-013-7051-7; pmid: 23974642
62. Y. Ando *et al*., Effects of tafamidis treatment on transthyretin (TTR) stabilization, efficacy, and safety in Japanese patients with familial amyloid polyneuropathy (TTR-FAP) with Val30Met and non-Val30Met: A phase III, open-label study. *J. Neurol. Sci.* **362**, 266–271 (2016). doi: 10.1016/j.jns.2016.01.046; pmid: 26944161
63. L. Bartalena, J. Robbins, Thyroid hormone transport proteins. *Clin. Lab. Med.* **13**, 583–598 (1993). doi: 10.1016/S0272-2712(18)30427-X; pmid: 8222576
64. M. J. Saraiva, P. P. Costa, D. S. Goodman, Biochemical marker in familial amyloidotic polyneuropathy, Portuguese type. Family studies on the transthyretin (prealbumin)-methionine-30 variant. *J. Clin. Invest.* **76**, 2171–2177 (1985). doi: 10.1172/JCI112224; pmid: 3908483
65. D. R. Jacobson *et al*., Variant-sequence transthyretin (isoleucine 122) in late-onset cardiac amyloidosis in black Americans. *N. Engl. J. Med.* **336**, 466–473 (1997). doi: 10.1056/NEJM199702133360703; pmid: 9017939
66. M. L. Soares *et al*., Haplotypes and DNA sequence variation within and surrounding the transthyretin gene: Genotype-phenotype correlations in familial amyloid polyneuropathy (V30M) in Portugal and Sweden. *Eur. J. Hum. Genet.* **12**, 225–237 (2004). doi: 10.1038/sj.ejhg.5201095; pmid: 14673473
67. T. Yokoyama, Y. Kosaka, M. Mizuguchi, Crystal structures of human transthyretin complexed with glabridin. *J. Med. Chem.* **57**, 1090–1096 (2014). doi: 10.1021/jm401832j; pmid: 24422526
68. C. E. Bulawa *et al*., Tafamidis, a potent and selective transthyretin kinetic stabilizer that inhibits the amyloid cascade. *Proc. Natl. Acad. Sci. U.S.A.* **109**, 9629–9634 (2012). doi: 10.1073/pnas.1121005109; pmid: 22645360
69. M. Sun, X. Zhang, H. Hao, W. Li, C. Lu, Nocarbenzoxazoles A–G, benzoxazoles produced by halophilic *Nocardiopsis lucentensis* DSM 44048. *J. Nat. Prod.* **78**, 2123–2127 (2015). doi: 10.1021/acs.jnatprod.5b00031; pmid: 26270803
70. D. Du *et al*., Genome engineering and direct cloning of antibiotic gene clusters via phage φBT1 integrase-mediated site-specific recombination in *Streptomyces*. *Sci. Rep.* **5**, 8740 (2015). doi: 10.1038/srep08740; pmid: 25737113
71. G. Wang *et al*., CRAGE enables rapid activation of biosynthetic gene clusters in undomesticated bacteria. *Nat. Microbiol.* **4**, 2498–2510 (2019). doi: 10.1038/s41564-019-0573-8; pmid: 31611640
72. J. R. Patel, J. Oh, S. Wang, J. M. Crawford, F. J. Isaacs, Cross-kingdom expression of synthetic genetic elements promotes discovery of metabolites in the human microbiome. *Cell* **185**, 1487–1505.e14 (2022). doi: 10.1016/j.cell.2022.03.008; pmid: 35366417
73. G. Muth, The pSG5-based thermosensitive vector family for genome editing and gene expression in actinomycetes. *Appl. Microbiol. Biotechnol.* **102**, 9067–9080 (2018). doi: 10.1007/s00253-018-9334-5; pmid: 30191290
74. F. Xie *et al*., Autologous DNA mobilization and multiplication expedite natural products discovery from bacteria, Version 4, Dryad (2024); https://doi.org/10.5061/dryad.2280gb60t.

ACKNOWLEDGMENTS

We thank the Helmholtz Institute for Pharmaceutical Research Saarland (HIPS) for use of the MS and NMR platforms. We also thank A. F. Stewart, A. Keller, C. Beemelmanns, and A. A. Gurevich for their valuable discussions. **Funding:** C.F. and R.M. acknowledge support from the Helmholtz International Lab (Helmholtz Association, InterLabs0007) and the German Federal Ministry of Education and Research (BMBF, 01DO22003). R.M. acknowledges funding from the German Research Foundation (DFG) and German Center for Infection Research (DZIF). **Author contributions:** Conceptualization: C.F., F.X., and R.M. Methodology: C.F., F.X., H.Z., and X.W. Investigation: C.F., F.X., H.Z., J.L., X.Y., M.N., A.A.A., A.K., J.H., and O.V.K. Visualization: C.F., F.X., H.Z., and X.W. Funding acquisition: C.F. and R.M. Project administration: C.F., R.M., and F.X. Supervision: C.F. and R.M. Writing – original draft: C.F., F.X., and H.Z. Writing – review and editing: C.F., F.X., R.M., H.Z., and X.W. **Competing interests:** The authors declare that they have no competing interests. **Data and materials availability:** All tool plasmids developed in this study will be deposited in Addgene (ID nos. 227507, 227508, and 227579 to 227583). All DNA sequences of TDRs have been deposited in GenBank under accession nos. OR339702 (*Sav11*), OR339701 (*Sar13*), and OR339703 (*Sav17*). All DNA sequences of ACTIMOT toolkit plasmids have been deposited in GenBank under accession nos. OR264833 (pRel-Hyg), OR264834 (pRel), OR264835 (pHelp), OR264836 (pCap-SG5-Hyg), OR264837 (pCap-SG5-Apr), OR264838 (pCap-101-Hyg), and OR264839 (pCap-101-Apr). The MS and NMR data for new molecules are deposited at Dryad (*74*). All other data supporting this study's findings are available in the main text and the supplementary materials.

SUPPLEMENTARY MATERIALS

Submitted 22 August 2023; accepted 10 October 2024
10.1126/science.abq7333